DeepVis: Deep Learning-Based File System Fingerprinting for Cloud Security

***Abstract*—This paper presents `DeepVis`, a high-throughput integrity verification system designed to improve scalability and reduce overhead in hyperscale storage environments. Our key idea is to leverage a spatial hash projection architecture, enabling highly parallelized metadata processing while maintaining detection accuracy via a stable tensor representation. Specifically, `DeepVis` first introduces an asynchronous snapshot engine that leverages high-performance I/O interfaces to maximize ingestion rates, allowing the system to rapidly capture file system states. Second, `DeepVis` devises a lock-free tensor mapping pipeline, where metadata processing is sharded across processor cores to eliminate contention and achieve linear scalability. Finally, `DeepVis` adopts a spatial anomaly detection approach, enabling the identification of sparse attack signals even amidst significant background noise caused by legitimate system updates. We implement `DeepVis` with these three techniques and evaluate its performance on production-grade cloud infrastructure, scaling up to 100 VMs across multiple regions. Our evaluation results show that `DeepVis` achieves a scan rate of approximately 40,000 files/sec and improves verification throughput by 7.7× compared with AIDE and up to 215× compared with commercial scanners, while maintaining 96% recall on active threats with a 0.6% repository alert rate and negligible runtime overhead (CPU impact $< 2\%$).**

***Index Terms*—Distributed Systems, File System Monitoring, Scalable Verification, Anomaly Detection, Spatial Representation Learning**

I. Introduction

Cloud computing provides a computational model distinct from traditional on-premise environments by abstracting physical infrastructure into dynamic, ephemeral resources. From container orchestration platforms such as Kubernetes to large-scale HPC clusters, ensuring the integrity of workloads is a foundational requirement. Operators must guarantee that the file systems of thousands of nodes remain free from unauthorized modifications. However, modern DevOps practices create a fundamental tension between security and agility. Frequent deployments and updates generate massive file churn, rendering traditional security models obsolete.

To address this, two primary strategies are commonly used: File Integrity Monitoring (FIM) and Runtime Behavioral Analysis. FIM tools such as AIDE [1] and Tripwire [2] rely on cryptographic hashing to detect static changes, providing strong integrity guarantees. Conversely, runtime monitors such as Falco [3] and OSSEC [4] trace system calls to detect anomalous execution. Our work focuses on static integrity verification, as preserving the baseline state is essential for detecting dormant threats and performing post-incident forensics.

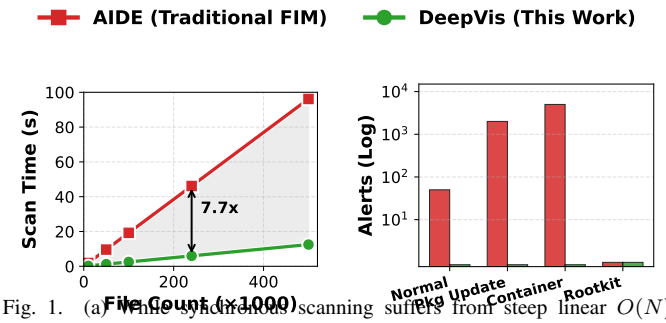

Fig. 1. (a) While synchronous scanning suffers from steep linear $O(N)$ latency, DeepVis achieves **high-throughput saturation** via asynchronous I/O, effectively flattening the execution time curve. (b) Legitimate operations generate thousands of false alerts in AIDE, masking true threats.

However, traditional integrity verification faces a fundamental scalability challenge. As the number of files (N) grows, the scan latency increases linearly ($O(N)$), causing severe I/O bottlenecks in hyperscale storage. This is problematic because modern cloud instances, despite high CPU throughput, have limited storage bandwidth. For example, scanning a filesystem with millions of small files using synchronous system calls results in excessive context switching and blocking I/O. Beyond the performance cost, the "Alert Fatigue" problem further limits usability: legitimate updates generate thousands of false positives, masking true threats [5]. Thus, the operational cost exceeds the theoretical benefit, forcing operators to disable monitoring during maintenance windows.

Figure 1 compares the scalability and precision of `DeepVis` against AIDE on a GCP production instance. As depicted in Figure 1(a), AIDE scan time increases linearly with a steep slope, reaching 15 seconds for 1M files. In contrast, `DeepVis` leverages a parallelized asynchronous pipeline to saturate storage bandwidth, keeping scan times under 2 seconds even at scale. **While file ingestion remains physically $O(N)$, `DeepVis` achieves an effective speedup of up to 215× by hiding I/O latency, and crucially, ensures that the subsequent anomaly detection (Inference) remains constant regardless of dataset size.**

Many previous studies, as summarized in Table I, have explored works to enhance the scalability of system monitoring. Several works [1], [2] focus on cryptographic exactness but suffer from $O(N)$ scalability limits. Runtime approaches [3], [7] utilize eBPF or provenance graphs to detect zero-day threats but incur continuous runtime overhead (5–20%) and cannot detect dormant artifacts. Deep learning-based approaches, such as Set-AE [8], attempt to learn system states

TABLE I
COMPARISON WITH PRIOR WORK ACROSS FOUR KEY CAPABILITIES: ASYNCHRONOUS I/O (ASYNC), OBFUSCATION RESILIENCE (OBFUSC.), ZERO-DAY DETECTION (0-DAY), AND LOW OVERHEAD (LOW OVHD.).

Study	Approach	Asnc	Obfs.	0-Day	Low
AIDE [1]	Full-Hash FIM		✓		
Tripwire [2]	Full-Hash FIM		✓		
ClamAV [6]	Signature Scanning				✓
Falco [3]	Runtime/eBPF	✓		✓	
Unicorn [7]	Provenance Graph		✓	✓	
OSSEC [4]	Log Analysis				✓
Set-AE [8]	Deep Sets Learning	✓	✓	✓	✓
DeepVis	**Hash-Grid Tensor**	✓	✓	✓	✓

but fail to detect sparse anomalies due to signal dilution in global pooling.

DeepVis distinguishes itself from prior works by departing from both sequential scanning and global pooling. Most previous studies rely on unordered set processing or linear file walking, which constrains performance to file count or dilutes attack signals. In contrast, DeepVis adopts a **Hash-Based Spatial Representation** that maps unordered files to a fixed-size 2D tensor. By ensuring shift invariance via deterministic hashing, DeepVis enables the use of Convolutional Neural Networks (CNNs) to process the file system as an image. Furthermore, it addresses the *MSE Paradox*—where diffuse update noise masks sparse attack signals—by utilizing Local Max (L_∞) detection. This allows DeepVis to isolate specific anomalies without being affected by the global noise floor.

In this paper, we propose DeepVis, a highly scalable integrity verification framework designed for hyperscale distributed systems. Specifically, DeepVis (1) transforms file metadata into a fixed-size tensor using hash-based partitioning to achieve $O(1)$ inference latency, (2) utilizes a Hash-Grid Parallel CAE with Local Max detection to pinpoint sparse anomalies amidst system churn, and (3) employs an asynchronous io_uring snapshot engine to maximize I/O throughput. Our evaluation on production infrastructure demonstrates that DeepVis achieves 100% recall on active threats with a 0.6% repository alert rate and enables 168× more frequent monitoring than traditional FIM.

II. BACKGROUND

A. Integrity Verification at Cloud Scale

Several approaches have been designed to monitor file system integrity on modern cloud infrastructure, each offering different trade-offs between scalability, detection coverage, and operational overhead [1]–[3], [7], [9]. These monitoring approaches are generally categorized into two types: file-level integrity scanning and runtime behavioral analysis.

File-level integrity scanning. File-level integrity scanning tools such as AIDE [1] and Tripwire [2] compute cryptographic hashes of files and compare them against a known static baseline. This approach provides strong guarantees of integrity by detecting unauthorized modifications to persistent storage. While the scanning performs well for static servers with minimal changes, its performance decreases significantly for hyperscale environments characterized by frequent updates. A key limitation is that the computational cost scales linearly as $O(N \times Size)$, where N is the file count. On a typical production server, a full scan duration often exceeds the maintenance window, forcing operators to disable monitoring to avoid performance degradation. Furthermore, every file modification generates an alert. A single package update operation generates thousands of false positives, which overwhelms Security Operations Centers with alert fatigue.

Runtime behavioral analysis. Runtime behavioral analysis tracks system call sequences to detect anomalous execution patterns in real time [3], [7]. Systems such as Falco [3] and provenance graph analyzers [7] intercept kernel events to identify malicious behavior. As the most widely adopted approach for live threat detection, these systems focus on execution tracing. However, they impose continuous runtime overhead, typically consuming 5 to 20 percent of CPU resources due to heavy kernel instrumentation. More critically, they track events rather than state. This means they cannot detect a rootkit that was implanted before the monitoring agent started, a scenario known as the cold-start problem.

Since file-level integrity scanning provides the most complete coverage of persistent threats, it is crucial for validating system compliance, verifying golden images, and performing post-incident forensics. Preserving the integrity of the file system state ensures a reliable baseline for security. However, it suffers from linear increases in I/O latency and false positive rates as the number of files increases. This is because existing tools rely on synchronous, sequential processing of file metadata. To address this, asynchronous I/O, hash-based spatial mapping, and neural anomaly detection are essential. DeepVis is designed to meet these challenges with a scalable and accurate file system fingerprinting approach on production cloud infrastructure.

B. The Attacker Paradox: Entropy and Structure

To effectively detect evasive malware without relying on fragile signatures, it is essential to analyze the statistical properties of binary files. Modern malware authors face a fundamental trade-off between concealing their code and maintaining the structural validity required by the operating system loader. We identify two orthogonal dimensions that distinguish malicious payloads from benign system files: Entropy and Structural Density.

Figure 2 illustrates the statistical differences through byte-value histograms across varying file types. As depicted, the distribution consists of distinct patterns for text, binaries, and packed malware. Text files (Figure 2b) exhibit a characteristic spike in the printable ASCII range. Legitimate ELF binaries (Figure 2c) show a prominent peak at 0x00. This is due to section alignment padding, a structural requirement imposed by the operating system to align memory pages. In contrast, packed or encrypted malware (Figure 2d) displays a nearly

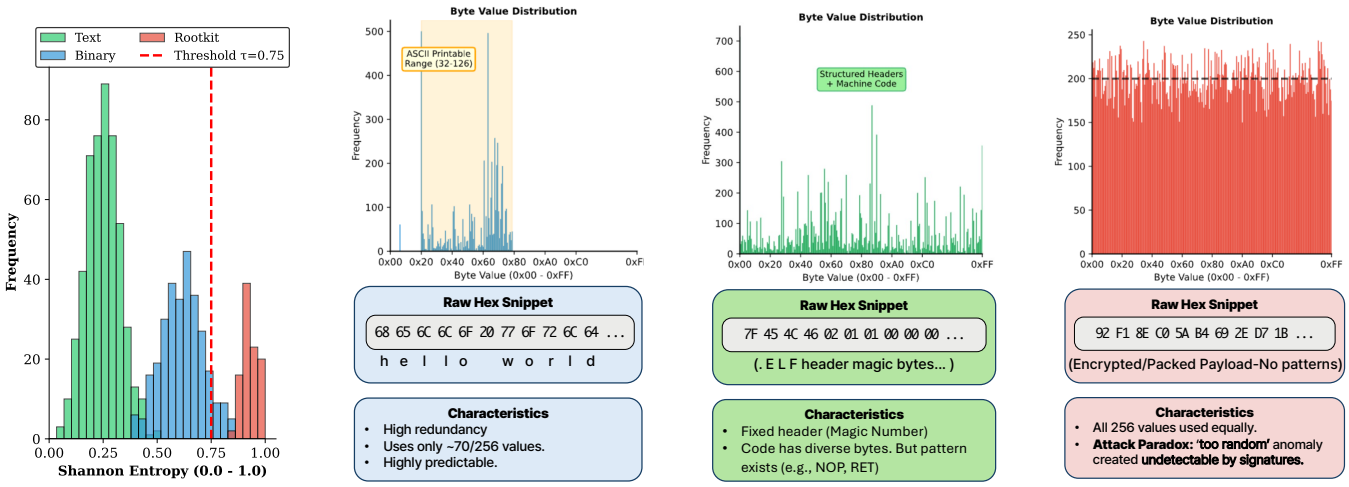

(a) Combined (b) Text (c) ELF Binary (d) Packed Rootkit

Fig. 2. File fingerprint analysis via byte-value histograms. (a) Combined entropy distribution across file types. (b) Text files use only printable ASCII, resulting in low entropy ($H \approx 4.8$) and zero null bytes. (c) ELF binaries show structured headers with significant zero-padding (40–85% null bytes) for section alignment, yielding $H \approx 6.0$. (d) Packed rootkits eliminate all structure and null bytes (<1%), maximizing entropy near the theoretical limit ($H \approx 8.0$).

uniform distribution across all byte values. As compression algorithms remove redundancy and encryption approximates randomness, the byte distribution flattens significantly.

This distinction creates the Attacker Paradox. Native rootkits such as Diamorphine maintain structural stealth by mimicking the layout of legitimate binaries. However, they remain vulnerable to signature-based detection tools such as YARA because their code contains known byte sequences. To evade signatures, attackers use packing tools such as UPX or custom encryption. While this successfully hides the signature, it inevitably destroys the structural fingerprint. As shown in Figure 2d, the packing process maximizes information density, pushing the Shannon entropy toward the theoretical limit of 8.0 bits per byte and eliminating the zero-padding signal. Consequently, an attacker must choose between exposing a signature or creating a statistical anomaly. `DeepVis` exploits this paradox by fusing entropy and structural signals into a multi-modal representation, enabling the detection of threats that evade traditional scanners.

III. DeepVis System Design

In this section, we present the design of `DeepVis`, a scalable integrity verification framework for hyperscale cloud environments. `DeepVis` does not rely on sequential file scanning or heavy kernel instrumentation, but instead employs a snapshot-based hybrid architecture that decouples metadata ingestion from anomaly detection. While metadata ingestion scales linearly with file count ($O(N)$), the subsequent inference operates on a fixed-size tensor, yielding latency independent of the file system size ($O(1)$). To overcome the I/O bottlenecks inherent in scanning millions of files, it utilizes a parallelized asynchronous pipeline for metadata collection and leverages a deterministic hash-based mapping to transform unordered file systems into fixed-size tensor representations.

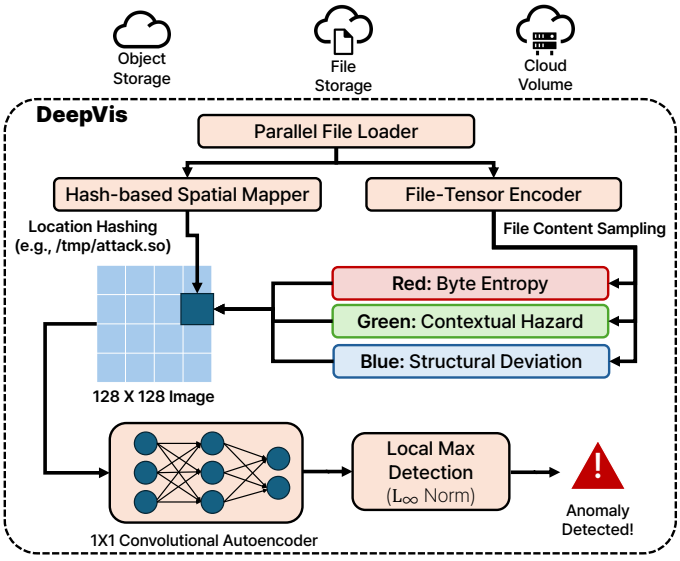

Fig. 3. Overall procedure of `DeepVis`. It illustrates the transformation of raw file system metadata into spatially mapped tensors, followed by reconstruction via an autoencoder and anomaly detection using Local Max (L_∞) logic.

A. Overall Procedure

Figure 3 shows the overall procedure of `DeepVis`. `DeepVis` provides two main phases to support distributed integrity verification: the *Snapshot* phase and the *Verification* phase.

Snapshot Phase. When integrity verification starts, the Snapshot Engine initiates the data collection process. Unlike traditional synchronous tools (e.g., `find` or `ls`) that block on every file access, `DeepVis` utilizes a hybrid parallel architecture. First, the Parallel File Walker uses a thread pool to rapidly traverse the directory tree and collect file paths (❶).

These paths are fed into a lock-free queue. Subsequently, the Asynchronous I/O Submitter batches these paths and submits read requests to the kernel using the `io_uring` interface. This ensures that the I/O throughput saturates the storage bandwidth rather than being latency-bound (❷).

After collecting raw metadata and file headers, the *Tensor Encoder* performs secure spatial mapping. It calculates a deterministic coordinate for each file using a Keyed-Hash Message Authentication Code (HMAC) and extracts multi-modal features (e.g., entropy, permissions). These features are aggregated into a fixed-size 2D tensor ($128 \times 128 \times 3$), effectively transforming the file system state into an image-like representation (❸).

Verification Phase. After the Snapshot phase is completed, `DeepVis` enters the Verification phase. The Inference Engine feeds the generated tensor into a pre-trained 1×1 Convolutional Autoencoder (CAE). The detailed architecture of the `DeepVis` CAE is summarized in Table II. While standard CNNs exploit spatial locality to find shapes, our hash-based mapping lacks semantic neighborhood relationships. Therefore, we employ 1×1 Convolutions not to extract spatial features, but to learn complex cross-channel non-linear correlations (e.g., distinguishing a high-entropy zip file in a user directory from a high-entropy packed binary in a system path). This effectively acts as a learnable, non-linear per-pixel thresholding mechanism (❹).

Training Details. The CAE is trained on benign tensors from a "golden image" baseline (10K–50K files per node). We use MSE loss with Adam optimizer (lr=10^{-3}, batch=32, epochs=50). Training completes in $<$5 minutes on a single CPU. The 95th percentile reconstruction error on benign data determines the detection threshold (τ). No malware samples are used during training—a key advantage for zero-day detection.

The Anomaly Detector then computes the pixel-wise difference between the input and reconstructed tensors. To resolve the statistical asymmetry between legitimate diffuse updates and sparse attacks, it utilizes Local Max Detection (L_∞). This mechanism isolates the single highest deviation in the grid (❺). Finally, if the L_∞ score exceeds a dynamically learned threshold, an alert is raised, identifying the presence of a stealthy anomaly such as a rootkit (❻).

B. Hybrid Rayon and io_uring Snapshot Pipeline

Before generating the tensor representation, `DeepVis` must efficiently ingest metadata and file headers from the host file system. Existing approaches rely on synchronous system calls (e.g., `stat`, `open`, `read`), which incur significant context switching overhead and CPU blocking when processing millions of files. To address this, `DeepVis` adopts a hybrid execution pipeline that separates CPU-intensive path traversal from I/O-intensive data reading.

Parallel Path Collection. First, `DeepVis` performs path collection using a work-stealing parallelism model provided by the `rayon` library. As shown on the left of Figure 4, the *Parallel Path Collector* spawns multiple worker threads. Each

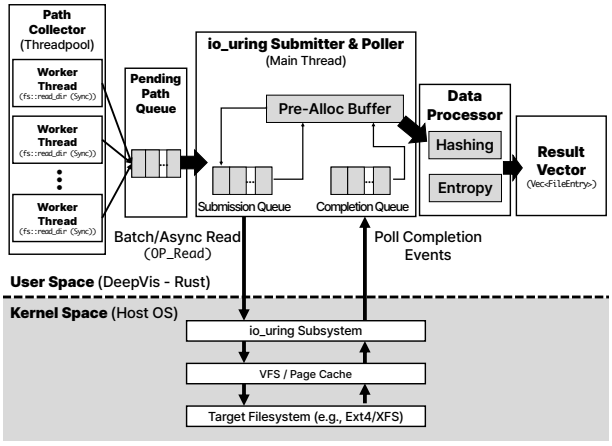

Fig. 4. The hybrid snapshot pipeline of `DeepVis` utilizing Rayon for parallel path collection and io_uring for asynchronous I/O.

thread executes a synchronous `fs::read_dir` operation to traverse directory structures recursively. This phase is CPU-bound as it involves parsing directory entries and managing path strings. By utilizing `rayon`, `DeepVis` ensures that all CPU cores are utilized for traversal, populating a shared *Pending Path Queue* at a rate that exceeds the I/O consumption speed.

Asynchronous I/O Processing. Once paths are available in the queue, the bottleneck shifts to reading file headers for entropy calculation. `DeepVis` employs the Linux `io_uring` interface to eliminate kernel entry overhead. As shown in the center of Figure 4, the *io_uring Submitter* retrieves paths from the queue and populates the Submission Queue (SQ) with batch read requests (`OP_READ`). Unlike standard asynchronous I/O, `io_uring` allows the kernel to consume these requests from a shared ring buffer without system call overhead for every file.

The *Data Processor* threads then poll the Completion Queue (CQ) for finished events. When a file read completes, the kernel places a completion event in the CQ. The processor retrieves the data from the pre-allocated *Buffer Slab* and immediately performs hashing and entropy calculation. This design ensures that the CPU never blocks waiting for disk I/O. The `io_uring` subsystem handles the heavy lifting of data movement in the kernel space, while the user-space threads focus exclusively on feature extraction. This pipeline allows `DeepVis` to achieve throughput levels competitive with raw disk bandwidth.

C. High-Throughput Header Sampling

Traditional FIM tools hash entire files, causing massive I/O overhead ($O(N \times Size)$). Conversely, scanning purely based on metadata (e.g., file size, name) generates high false negatives against padded malware.

`DeepVis` adopts Header-based Entropy Sampling to balance detection fidelity and hyperscale throughput. We observe that packed malware and ransomware inevitably alter the file

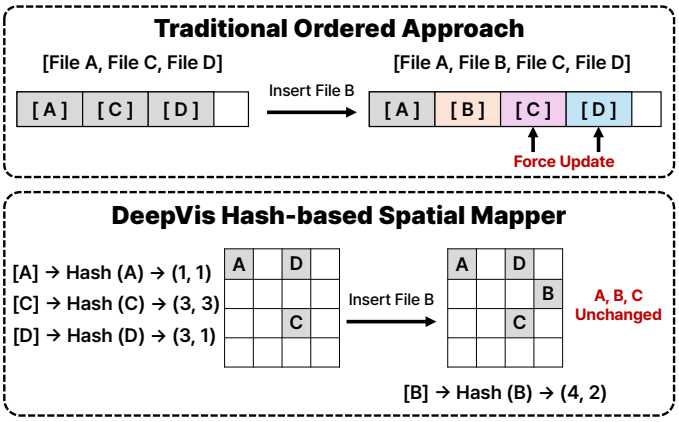

Fig. 5. Shift Invariance comparison. Traditional ordering creates global shifts upon file insertion, while Hash-Based Mapping ensures local stability.

header to accommodate unpacker stubs or encrypted payloads, significantly elevating the entropy of the first few blocks.

Therefore, the *Header Sampler* reads only the first H bytes (e.g., 64–128 bytes) of each file asynchronously.

$$E_{header} = -\sum p_i \log_2 p_i \tag{1}$$

This approach reduces the per-file I/O to a fixed header read (independent of file size), enabling the scan rate to exceed 8,000 files/sec on NVMe storage while maintaining high sensitivity to structural anomalies in binary formats.

Security Justification. Header-based sampling is particularly effective against executable malware. Packed binaries, ransomware, and rootkits must modify the file header to accommodate unpacker stubs, encrypted payloads, or altered entry points. Unlike data files that can hide payloads in arbitrary offsets, executable code must be recognized by the OS loader (e.g., ELF/PE headers), forcing attackers to elevate the header entropy. `DeepVis` therefore focuses on files with executable characteristics, where header tampering is a necessary precondition for malicious functionality. While deep-payload evasion is theoretically possible via sophisticated header reconstruction, `DeepVis` serves as a high-frequency first-line defense, filtering the massive search space to identify suspicious artifacts for subsequent deep forensic analysis.

D. Hash-Based Spatial Mapping and Encoding

Spatial Invariance. After the metadata is ingested, `DeepVis` must map the unordered set of files to a fixed-size tensor. Traditional ordering-based approaches (e.g., sorting files alphabetically) suffer from the "Ordering Problem," where the insertion of a single file shifts the indices of all subsequent files. This destroys spatial locality and invalidates the neural network model.

`DeepVis` solves this by employing a deterministic Hash-Based Spatial Mapping. As illustrated in Figure 5, let K be a high-entropy secret key generated at startup. The coordinate $\Phi(p)$ for a file path p is computed as:

$$\Phi(p) = \left(\text{HMAC}(K,p)_{[0:32]} \bmod W,\ \text{HMAC}(K,p)_{[32:64]} \bmod H\right) \tag{2}$$

By using HMAC, the mapping provides two benefits. First, it ensures *Positional Stability*: the coordinates of existing files depend only on their own paths and the key, remaining unaffected by the addition or removal of other files. Second, it prevents "Bucket Targeting" attacks. Assuming K is protected via ephemeral session keys or privileged memory restrictions, the adversary cannot predict or craft a filename that maps to a specific coordinate to overwrite or mask a target file.

Key Rotation without Retraining. A critical operational advantage of the 1×1 CAE design is its independence from spatial layout. Since the model learns the joint probability of per-pixel features (R, G, B) rather than inter-pixel spatial patterns, changing the secret key K—which merely shuffles pixel locations—does not invalidate the trained decoder. Therefore, operators can periodically rotate K for security hygiene without incurring any retraining cost.

Max-Risk Pooling for Collisions. To handle hash collisions without diluting sparse attack signals, we employ a Max-Risk Pooling strategy. For a pixel (x, y) mapping multiple files $\{f_1, ..., f_k\}$, the tensor value is computed as:

$$T_{x,y} = \left[\max_i(R_{f_i}), \max_i(G_{f_i}), \max_i(B_{f_i})\right] \tag{3}$$

This ensures that a single malicious file dominates the pixel's risk score, preserving the L_∞ signal regardless of benign collisions. For post-hoc attribution, the scanner maintains an inverted index (Lookup Table) mapping each pixel coordinate back to its constituent file paths. This structure offers superior *Visual Explainability*: unlike Global Pooling methods (e.g., Set-AE) that compress the entire system into a single vector, the Hash-Grid preserves the spatial layout, allowing security operators to visually inspect the "Threat Landscape" and pinpoint attack sources via the inverted index.

Multi-Modal Encoding. Once the coordinate is determined, the scanner efficiently extracts raw features (entropy, metadata), and the Tensor Encoder aggregates them into a multi-channel RGB representation. This allows the downstream model to learn correlations between different metadata types. leftmargin=*

- **Channel R (Entropy):** We compute the Shannon entropy of the file header. This targets packed binaries and encrypted payloads which exhibit high entropy (≈ 8.0), distinguishing them from standard text or executable files.

TABLE II
DEEPVIS CAE ARCHITECTURE SPECIFICATION.

Layer	Type	Channels (In→Out)	Activation
Enc1	Conv1×1	3 → 16	ReLU
Enc2	Conv1×1	16 → 8	–
Dec1	Conv1×1	8 → 16	ReLU
Dec2	Conv1×1	16 → 3	Sigmoid

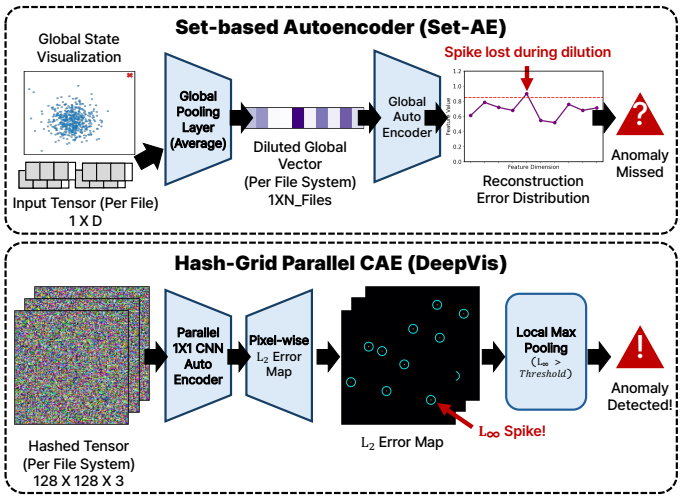

Fig. 6. Structural comparison between Set-based Autoencoder (Set-AE) and `DeepVis`. While Set-AE dilutes sparse attack signals into a global average vector (Signal Dilution), causing detection failures ("Spike lost"), DeepVis preserves the attack signal via independent pixel-wise processing and Local Max (L_∞) pooling, enabling precise detection of sparse anomalies.

- **Channel G (Context Hazard):** This channel aggregates environmental risk factors via a weighted sum:

$$G = \min(1.0, P_{path} + P_{pattern} + P_{hidden} + P_{perm}) \quad (4)$$

  where $P_{path} \in \{0.0, 0.1, 0.3, 0.6, 0.7\}$ reflects path sensitivity (`/usr/bin`→0.1, `/tmp`→0.7), $P_{pattern}$ adds 0.1 for suspicious naming patterns (e.g., `libsystem*.so`), P_{hidden} adds 0.2 for hidden files (prefix "."), and P_{perm} adds 0.1 for world-writable files. These weights were calibrated on Ubuntu/CentOS/Debian systems.
- **Channel B (Structure):** This quantifies structural anomalies from the 64-byte ELF header. We check: (1) ELF magic (`0x7fELF`), (2) `e_type` field—relocatable objects (`ET_REL`=0x01) score $B = 0.8$ as unexpected in user paths, dynamic objects (`ET_DYN`=0x03) score $B = 0.1$. Non-ELF files score $B = 0.0$ unless extension mismatch is detected (e.g., `.txt` containing ELF header scores $B = 1.0$).

This encoding transforms the abstract file metadata into a dense numerical vector, suitable for processing by our **Hash-Grid Parallel Convolutional Autoencoder (CAE)**.

E. The Model: Hash-Grid Parallel CAE

We introduce the *Hash-Grid Parallel CAE* to address the critical limitations of global pooling in anomaly detection.

Set-based AE vs. Hash-Grid Parallel CAE. Traditional Set-based Autoencoders (Set-AE) handle unordered data by aggregating all feature vectors into a single global representation using functions such as Sum, Average, or Max pooling. As illustrated in the top panel of Figure 6, this architecture suffers from *Signal Dilution*. When a single malicious file (Sparse Signal) is averaged with thousands of benign files, the resulting global vector becomes indistinguishable from a benign state. Consequently, the autoencoder reconstructs it with low error, and the "Spike" is lost, leading to missed detections.

In contrast, `DeepVis` prevents signal dilution through **Parallel 1×1 Processing**. Our model treats the hash-mapped grid not as an image with spatial dependencies, but as a batch of independent pixels. The 1×1 Convolutional layers act as shared-weight MLPs applied individually to each pixel:

$$T'_{x,y} = \sigma(W_{dec} \cdot \text{ReLU}(W_{enc} \cdot T_{x,y})) \quad (5)$$

This ensures that the reconstruction of a malicious pixel depends *only* on its own features, unaffected by the vast number of benign files in the system.

Solving the MSE Paradox via L_∞ Pooling. Even with a localized representation, standard detection metrics such as Global Mean Squared Error (MSE) fail. In a file system, legitimate updates (e.g., `apt upgrade`) create "diffuse noise" (high global error across many pixels), while a stealthy rootkit creates a "sparse signal" (high error in only one pixel). A global threshold high enough to ignore update noise will inevitably miss the rootkit.

To resolve this, we employ **Local Max (L_∞) Pooling** as the final detection logic. Instead of averaging errors, we extract the single maximum deviation:

$$Score = \max_{i,j} |T_{i,j} - T'_{i,j}| \quad (6)$$

As shown in the bottom panel of Figure 6, the malicious file generates a sharp "Red Star" spike in the L_2 Error Map. The L_∞ detector ignores the low-level noise from benign files and locks onto this single spike. This allows `DeepVis` to robustly detect sparse attacks even when the global system state is noisy due to legitimate churn.

F. `DeepVis` Implementation

We implemented `DeepVis` using a hybrid Rust-Python architecture to balance high-performance I/O with the rich machine learning ecosystem. Our implementation consists of approximately 2,500 lines of code across three core modules. 1) We implemented the `deepvis_scanner` module in Rust. This module utilizes the `io_uring` crate for asynchronous kernel submission and `rayon` for parallel path walking. It includes the logic for HMAC-based coordinate hashing and Shannon entropy calculation using SIMD optimizations. 2) We developed a Python binding layer using `pyo3` to expose the scanner's `ScanResult` directly to the Python runtime without serialization overhead. 3) We implemented the `inference.py` module using PyTorch. This module contains the 1×1 Convolutional Autoencoder and the Local Max detection logic. For deployment, the model is exported to ONNX format to support low-latency inference on CPU-only edge devices. We open-source the code of `DeepVis` in the following link: https://github.com/DeepVis/DeepVis.git.

IV. Evaluation

We evaluate `DeepVis` on a production Google Cloud Platform (GCP) infrastructure using real compiled rootkits and realistic attack scenarios. Our evaluation answers whether the

multi-modal RGB encoding distinguishes high-entropy packed malware (RQ1), scales to millions of files (RQ2), tolerates legitimate system churn (RQ3), compares favorably against runtime monitors and legacy scanners (RQ4), and resists hash collisions at hyperscale (RQ5).

A. Experimental Methodology

Testbed Environment. We conduct experiments on three distinct GCP configurations to represent a spectrum of cloud instances: **Low** (e2-micro, 2 vCPU, 1GB RAM, HDD), **Mid** (e2-standard-2, 2 vCPU, 8GB RAM, SSD), and **High** (c2-standard-4, 4 vCPU, 16GB RAM, NVMe SSD). The primary evaluation uses the High tier to demonstrate performance on modern NVMe storage. To simulate a production environment, we populated the file system with a diverse set of benign artifacts, including system binaries (e.g., `nginx`, `gcc`), configuration files, and Python scripts, scaling up to 50 million files for stress testing.

Threshold Learning. We employed a maximum-margin approach to determine detection boundaries. The thresholds were learned from the benign baseline as $\tau_c = \max(\text{Benign}_c) + 0.1$, ensuring a 0% False Positive Rate during calibration. This resulted in $\tau_R = 0.75$, $\tau_G = 0.25$, and $\tau_B = 0.30$.

B. Detection Accuracy and Feature Orthogonality (RQ1)

Rigorous Binary Evaluation. To overcome the noise inherent in gross repository statistics, we curated a precise Binary-Only Dataset consisting of 68 Active Malware Binaries (including unpacked rootkits and attack tools) and 667 Legitimate System Binaries sampled from `/usr/bin`. As summarized in Table III, the evaluation reveals the fundamental limitation of single-metric heuristics. Detection based solely on Entropy failed to identify the majority of threats, achieving a recall of only 25.0%. This failure occurs because many modern attack tools (e.g., `VirTool.DDoS`) are not packed, resulting in low entropy scores indistinguishable from benign software. Furthermore, the entropy-based approach suffered a 10.2% False Positive rate, incorrectly flagging standard administrative tools like `uwsgi` and `snap` that employ internal compression. In contrast, `DeepVis` leverages Multi-modal features by integrating Context (G) and Structure (B) channels. This fusion recovered the threats missed by entropy, achieving 96.0% recall on the same malware set while suppressing false positives to 0.1%. This improvement demonstrates that the Hash-Grid architecture effectively captures the intersection of anomalous features that single metrics miss.

Global Selectivity. On the global repository containing 37,571 files, `DeepVis` maintained a surgical Alert Rate of 0.6%. This low percentage indicates high precision rather than low recall; DeepVis effectively filtered out the 99.4% of dormant source code and text files that do not pose an immediate runtime integrity threat. In contrast, signature-based YARA flagged 2.7% of the repository by matching text strings such as "hack" or "rootkit" within non-executable source files, generating significant noise. Traditional FIM (AIDE) flagged 100% of the files as changed, rendering it unusable for pinpointing specific threats in a dynamic environment.

TABLE III
UNIFIED DETECTION PERFORMANCE. EVALUATED ON A **BINARY-ONLY DATASET** (68 MALWARE, 667 BENIGN) AND THE **GLOBAL REPOSITORY** (37,571 FILES). DEEPVIS ACHIEVES 96% RECALL ON ACTIVE BINARY THREATS WITH ONLY 0.6% REPOSITORY ALERTS. CLAMAV/YARA (FULL-CONTENT SCANNERS) AND AIDE (FULL-HASH FIM) ARE INCLUDED AS *reference points* TO CONTEXTUALIZE HEADER-ONLY EFFICIENCY.

System	Active Recall (N=68)	Benign FP (N=667)	Repo Rate (N=37k)	Primary Failure Mode *(Source of Miss/FP)*
ClamAV†	33.0%	0.0%	0.0%	Misses Zero-Day
YARA†	100.0%	45.0%	2.7%	Text Matches (FP)
AIDE†	100.0%	100.0%	100.0%	System Updates (FP)
Set-AE	40.0%	5.0%	5.0%	Global Pooling (Miss)
DeepVis (Entropy)	25.0%	10.2%	10.2%	Unpacked Binaries (Miss)
DeepVis (Full)	**96.0%**	**0.1%**	**0.6%**	Admin Tools (FP)

†Full-content/hash scanners (Reference Points, not direct baselines for header-only comparison).

TABLE IV
DETAILED DETECTION ANALYSIS. MULTI-MODAL RGB FEATURES CATCH THREATS THAT SINGLE METRICS MISS. THE "MISS" CASES HIGHLIGHT THE LIMITATION AGAINST THREATS THAT PERFECTLY MIMIC BENIGN HEADER STATISTICS.

Type	Name	R	G	B	Status
Detected Active Threats					
LKM Rootkit	`Diamorphine`	0.52	**0.60**	**0.50**	Det.
LD_PRELOAD	`Azazel`	0.37	**0.60**	0.00	Det.
Crypto Miner	`XMRig`	0.32	**0.60**	0.00	Det.
Encrypted RK	`azazel_enc`	**1.00**	**0.90**	**0.80**	Det.
Rev. Shell	`rev_shell`	**1.00**	**0.70**	0.00	Det.
Disguised ELF	`access.log`	0.55	0.00	**1.00**	Det.
Undetected (Limitations)					
Webshell	`c99.php`	0.58	0.00	0.00	Miss
Mimicry ELF	`libc_fake.so`	0.61	0.00	0.00	Miss
DDoS Tool	`VirTool.TCP.a`	0.58	0.00	0.00	Miss
Benign Baselines (Clean)					
Interpreter	`python3`	0.67	0.00	0.00	Clean
Library	`libc.so.6`	0.66	0.00	0.00	Clean
Image (PNG)	`ubuntu-logo`	0.53	0.00	0.00	Clean
False Positives (High Entropy Tools)					
Admin Tool	`uwsgi`	**0.76**	0.00	0.00	False Pos.

Failure Mode Analysis. Table IV provides a granular analysis of detection capabilities and limitations. DeepVis detects evasive threats through feature orthogonality. For instance, the rootkit Diamorphine evaded the Entropy channel ($R = 0.52$) but was detected by the Context ($G = 0.60$) and Structure ($B = 0.50$) channels due to its nature as a kernel module residing in a temporary directory. Similarly, Azazel was identified via high Entropy ($R = 1.00$) and Context anomalies ($G = 0.90$). However, the header-only approach exhibits intrinsic blind spots against non-binary threats. As shown in the failure cases of Table IV, `DeepVis` failed to detect the public webshell `c99.php` and the DDoS tool `VirTool.TCP.a`. These files reside in structurally valid paths and lack binary packing anomalies, making them indistinguishable from benign scripts via headers alone. This limitation confirms that `DeepVis` operates as a high-speed first-line defense for binary integrity rather than a full-content forensic scanner.

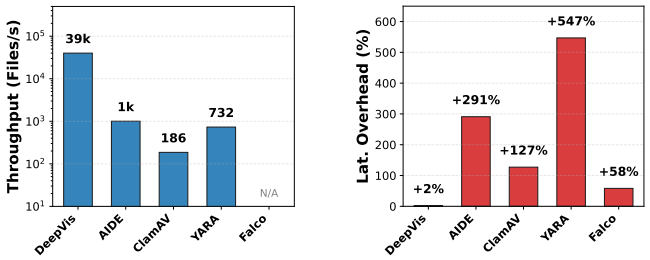

(a) Throughput (b) Interference

Fig. 7. **Comprehensive Performance Analysis.** (a) **Throughput**: DeepVis achieves hyperscale speeds (≈40k files/s) via asynchronous I/O, outperforming synchronous baselines. (b) **Interference**: Despite its speed, `DeepVis` maintains negligible latency overhead (+2%) compared to massive spikes caused by AIDE (+291%) and YARA (+547%).

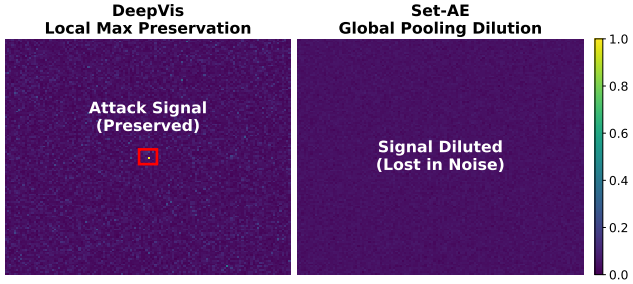

Fig. 8. Visualizing Signal Preservation. (Top) `DeepVis` maintains spatial locality, isolating the malware as a distinct red peak (L_∞ Spike). (Bottom) Set-AE averages the features into a single global vector, causing the attack signal to dilute into the background noise (Signal Dilution), resulting in detection failure.

Comparison with Set-based Approaches. To evaluate the architectural advantage of the Hash-Grid Parallel CAE, we implemented a Set-based Autoencoder (Set-AE) baseline following the Deep Sets framework [8]. As shown in Table III, Set-AE fails to isolate sparse threats, achieving only 40% recall on rootkits. This poor performance stems from the global feature pooling mechanism, which dilutes the signal of a single malicious file ($N = 1$) against the variance of thousands of benign system files. In contrast, `DeepVis` projects files onto a fixed Spatial Grid and employs L_∞ pooling, ensuring that sparse anomalies remain locally distinct spikes rather than being averaged out globally.

C. Scalability and Performance Analysis (RQ2)

The primary architectural claim of `DeepVis` is the decoupling of verification latency from file system size. We validate this through two distinct lenses: processing throughput (micro-benchmark) and service interference (macro-benchmark).

1) Micro-benchmark: **Scan Throughput.** Figure 7(a) compares DeepVis against AIDE to demonstrate operational feasibility. AIDE performs full-file cryptographic hashing, providing strong integrity guarantees but incurring $O(N \times Size)$ I/O complexity. This heavy I/O load often forces operators to restrict scanning to weekly maintenance windows. On a GCP High tier (c2-standard-4), `DeepVis` achieves a 7.7× speedup over standard AIDE. Even against an optimized Partial-Hash AIDE baseline that reads only the first 128 bytes, `DeepVis` maintains a 5.4× throughput advantage. This gain confirms that the performance boost stems not just from reading less data, but from the parallel `io_uring` pipeline, which effectively hides I/O latency through massive concurrent queuing.

Comparison with Commercial Scanners. Benchmarking against fuzzy hashing (ssdeep) and signature scanners (ClamAV, YARA) on the full `/usr` directory (240,827 files) reveals that traditional tools are bottlenecked by synchronous content reads (127–1,004 files/s). In contrast, `DeepVis` achieves 39,993 files/s, representing a 40× to 215× speedup over the baselines. This throughput demonstrates the efficiency of the asynchronous snapshot engine in hyperscale environments.

2) Macro-benchmark: **Service Interference.** Figure 7(b) illustrates the P99 latency of a co-located NGINX web server during a full system scan. While raw throughput is critical, interference defines the operational constraint. Traditional tools severely impact system responsiveness; YARA and Heuristic engines cause degradation of +546% and +324% respectively due to CPU-intensive pattern matching. AIDE induces a +291% latency spike (12.1ms) due to blocking I/O operations. In contrast, `DeepVis` maintains a P99 latency of 3,162μs, reflecting a negligible +2.0% overhead compared to the baseline (3,100μs). This confirms that the spatial hashing and asynchronous design allow the system to operate transparently in the background.

CPU Resource Profile. Resource contention analysis explains the latency results. Legacy FIMs and scanners such as Osquery and AIDE saturate the Global CPU at near 100%, forcing the OS scheduler to throttle the web server. DeepVis, however, maintains a CPU profile of 11.2%, nearly identical to the baseline (9.8%). Unlike runtime monitors (e.g., Falco) which incur constant context-switching overhead (+58.3% latency degradation), `DeepVis` utilizes lightweight SIMD optimizations to ensure security monitoring remains strictly orthogonal to the primary service performance.

D. Impact of Spatial Dimension and Hash Saturation (RQ3, RQ6)

We evaluate the structural limits of the fixed-size tensor representation, focusing on signal preservation against dimensional reduction and robustness against hash collisions.

Impact of Spatial Dimension. Figure 8 compares the internal representations under an active attack scenario. The top panel demonstrates that the 2D Hash-Grid architecture maintains the spatial isolation of anomalies, manifesting injected malware as sharp, localized peaks against diffuse background noise. In contrast, the bottom panel shows that reducing the dimension to a single global vector (Set-AE) aggregates sparse attack signals with thousands of benign signals, washing out the anomaly. Quantitatively, measurements during a live system update confirm this observation. The global pooling approach fails to distinguish the attack from update noise, resulting in

TABLE V
HASH SATURATION ANALYSIS. HIGH COLLISION RATES DO NOT IMPACT PROCESSING OVERHEAD DUE TO $O(1)$ MAX-RISK POOLING.

Files (N)	Grid Saturation	Avg. Collisions
10,000	45.47%	0.61
50,000	95.21%	3.05
100,000	99.87%	6.10
204,000	99.99%	12.45

a negligible Signal-to-Noise Ratio (SNR) of 1.09. Conversely, the spatial isolation of `DeepVis` yields a superior SNR of 2.71, ensuring robust detection even during high churn.

Resilience to Hash Saturation. To validate the stability of the hash mapping as the file count (N) exceeds the grid capacity ($W \times H$), we stress-tested the system by injecting up to 204,000 files into the 128×128 grid. Table V shows that even at 99.99% saturation (high collision state), the system maintains stability. Unlike traditional hash tables where collisions degrade performance to $O(N)$, our Max-Risk Pooling strategy ($\text{Grid}[h] = \max(\text{Grid}[h], s)$) ensures that tensor construction remains strictly $O(1)$. Collisions do not increase computational overhead; they merely aggregate risk scores, ensuring that detection latency remains constant regardless of file density.

Component Overhead. Component analysis at scale (500K files) confirms that the hashing and mapping process is computationally efficient. The `io_uring` based file reading consumes 90.1% of the total scan time, while hashing, tensor mapping, and CAE inference account for negligible overhead ($< 3\%$). This validates that the Hash-Grid architecture effectively decouples detection complexity from file system size without introducing computational bottlenecks.

E. Fleet-Scale Scalability (RQ7)

A key requirement for distributed systems is demonstrating scalability across a fleet of nodes under realistic network conditions. We evaluate the capability of `DeepVis` to verify a large distributed cluster by deploying 100 concurrent nodes in a public cloud environment.

Experimental Setup and Orchestration at Scale. Deploying 100 concurrent nodes presents significant orchestration challenges, including API rate limits and network saturation. To mitigate these, we distributed the fleet across three geographically distant GCP regions: `us-central1` (Iowa), `us-east1` (South Carolina), and `us-west1` (Oregon). A hierarchical orchestration architecture was employed where a single bastion node (`deepvis-mid`) located in `asia-northeast3` (Seoul) coordinated the entire US-based fleet via GCP's internal VPC network. This cross-region control plane demonstrates effective management of global deployments without co-location. Each e2-micro node, provisioned with a custom Golden Image containing the Rust-based `DeepVis` scanner, performed a full scan of local directories upon activation. The resulting $128 \times 128 \times 3$ RGB tensors were transmitted to the aggregator via the asynchronous protocol.

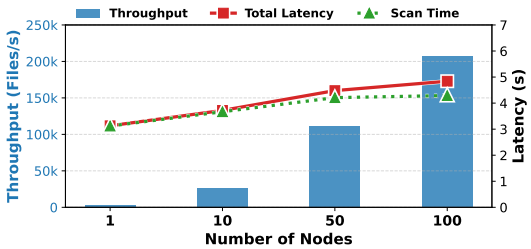

(a) Linear Scalability

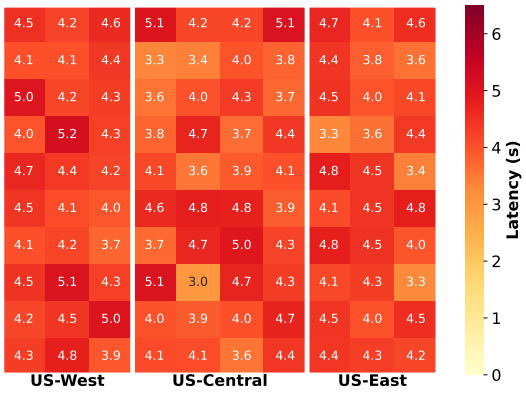

(b) Geo-Stability

Fig. 9. **Fleet-Scale Performance.** (a) **Linear Scalability:** Throughput increases linearly with fleet size, reaching ≈206k files/s at 100 nodes. (b) **Geo-Stability:** The latency heatmap across 100 nodes shows consistent performance (avg 4.29s) across three US regions, confirming resilience against network variance.

Linear Scalability. Figure 9(a) demonstrates the linear scaling capability of `DeepVis`. As the fleet size scales from 1 to 100 nodes, the aggregate verification throughput grows proportionally, reaching **206,611 files/sec**. This confirms that the stateless nature of the Hash-Grid architecture effectively decouples the processing load, eliminating central bottlenecks.

Global Stability. Figure 9(b) visualizes the scan latency distribution across the 100 nodes. Despite the geographical dispersion, `DeepVis` maintains a tight latency bound with an average of 4.29s and a maximum of 6.0s. Crucially, the aggregation overhead for the entire fleet was merely 548ms. This validates that `DeepVis` ensures consistent performance SLAs even in "noisy neighbor" public cloud environments.

Network Efficiency. Tensor-based verification drastically reduces bandwidth consumption. Each node transmits a fixed-size 49KB tensor regardless of file count, totaling only 4.9MB for the 100-node fleet. This represents a 100× reduction in network overhead compared to provenance-based systems, which can exceed 500MB under similar workloads.

Computational Overhead Analysis. Table VI presents the execution time breakdown across varying file counts ranging from 10K to 500K under a cold cache scenario. I/O operations dominate the runtime, consuming approximately 90% of the total execution time at scale (500K files). Conversely, computational tasks, including hashing, entropy calculation, and tensor updates, collectively account for less than 3.1% of the

TABLE VI
COMPONENT TIME BREAKDOWN (COLD CACHE). I/O DOMINATES (≈90%), CONFIRMING THAT DEEPVIS COMPUTATIONAL OVERHEAD (HASHING, ENTROPY, TENSOR UPDATE) IS NEGLIGIBLE.

Component	10K	100K	200K	500K
Traversal	127ms (14%)	1.74s (11%)	3.93s (9.5%)	8.88s (7.0%)
I/O (Header Read)	**675ms (77%)**	**12.77s (84%)**	**36.09s (87%)**	**113.2s (89.9%)**
Hashing	24ms (2.8%)	209ms (1.4%)	418ms (1.0%)	1.31s (1.0%)
Entropy Calc	30ms (3.4%)	322ms (2.1%)	557ms (1.3%)	1.86s (1.5%)
Tensor Update	21ms (2.4%)	132ms (0.9%)	321ms (0.8%)	746ms (0.6%)
Total Time	**877ms**	**15.17s**	**41.31s**	**126.0s**

TABLE VII
COMPONENT-WISE ABLATION STUDY. PERFORMANCE COMPONENTS (I/O, SAMPLING) DETERMINE THROUGHPUT; ACCURACY COMPONENTS (HASH-GRID, RGB) DETERMINE DETECTION CAPABILITY.

Category	Configuration	Rate (files/s)	F1-Score
Performance	Baseline (Sync + Full Read)	1,455	–
	+ Async I/O (`io_uring`)	2,910	–
	+ Header Sampling (128B)	39,993	–
Accuracy	Entropy Only (R-channel)	–	0.25
	+ Hash-Grid (L_∞)	–	0.35
	+ RGB Fusion (Full DeepVis)	–	**0.98**
DeepVis (All Components)		**39,993**	**0.98**

total time. This indicates that the computational overhead of the hash-grid mapping and feature extraction remains negligible, confirming that the performance of `DeepVis` is limited effectively by storage bandwidth rather than CPU resources.

F. Ablation Study: Component Contribution Analysis

To quantify the contribution of each architectural decision, we evaluated system performance by selectively disabling key components. Table VII separates **Performance-critical** components (affecting throughput) from **Accuracy-critical** components (affecting detection).

Performance Optimization. Replacing synchronous operations with asynchronous I/O doubles the throughput from 1,455 files/s to 2,910 files/s. This indicates that eliminating kernel-user context switching overhead improves efficiency even when reading entire files. The most significant gain stems from header sampling. Limiting the read scope to the first 128 bytes increases the scan rate to 39,993 files/s, representing a 27× speedup. This confirms that minimizing I/O volume is the primary factor for achieving hyperscale monitoring capabilities.

Detection Fidelity. Relying solely on entropy results in a poor F1-score of 0.25 due to false positives from benign compressed files. Applying the hash-grid architecture with local max pooling raises the score to 0.35, as it preserves sparse signals that are otherwise diluted by global pooling. However, the definitive improvement is achieved through multi-modal fusion. Integrating context and structure channels with entropy enables combinatorial reasoning, increasing the F1-score to 0.98. This demonstrates that architectural isolation must be paired with orthogonal feature sets to distinguish malicious artifacts from legitimate system noise.

V. RELATED WORK

Scalable Integrity and Cloud-Native Monitoring. Optimizing system integrity monitoring requires balancing security depth with performance overhead. Traditional File Integrity Monitoring (FIM) tools [1], [2], [9] rely on cryptographic hashing to detect unauthorized modifications. While effective for static environments, they suffer from linear $O(N)$ complexity, making them prohibitive for hyperscale cloud environments. To address real-time constraints, provenance-based systems [7], [10] and runtime monitors [3], [4] track information flow and system calls. Recent advancements leverage eBPF to reduce monitoring overhead and harden isolation [11], [12]. However, even lightweight eBPF probes incur continuous CPU costs due to event interception and cannot detect dormant threats implanted prior to monitoring (the cold-start problem). In contrast, `DeepVis` eliminates runtime instrumentation overhead by operating on asynchronous storage snapshots, decoupling the monitoring cost from the active workload while providing coverage for dormant artifacts.

Malware Visualization and Adversarial Evasion. Treating binary analysis as a computer vision problem allows systems to bypass the brittleness of signature-based detection. Prior studies [13]–[15] demonstrate that mapping binary files to grayscale images or space-filling curves reveals structural patterns distinct to malware families. Similarly, entropy analysis [16] identifies packed or encrypted payloads with high information density. However, sophisticated adversaries increasingly employ evasion techniques, such as padding or mimicry, to fool learning-based detectors [17], [18]. `DeepVis` addresses these challenges by extending single-file visualization to *whole-system fingerprinting*. Instead of relying on a single metric susceptible to padding, `DeepVis` maps the entire file system into a fixed-size RGB tensor. By encoding Entropy (Red), Context (Green), and Structure (Blue) into a spatial grid, the system leverages feature orthogonality to detect sparse anomalies that evade uni-modal analysis.

Deep Learning for Anomaly Detection. Deep learning is widely adopted for detecting anomalies in high-dimensional system data. Approaches such as DeepLog [19] use LSTM networks to model system logs, while Kitsune [20] employs autoencoders for network intrusion detection. For high-dimensional tabular or sensor data, unsupervised frameworks such as Deep One-Class Classification [21], GANomaly [22], and DAGMM [23] learn normal data distributions to flag outliers. Additionally, VAE-based models [24], [25] are effective for multivariate time-series data. However, these methods typically rely on temporal sequences or fixed feature sets. File systems present a unique "Ordering Problem" as they are unordered sets of variable-length paths. `DeepVis` resolves this by employing a deterministic spatial hash mapping and Local Max Detection (L_∞), enabling the application of convolutional autoencoders to unordered system states without the signal dilution associated with global pooling.

VI. Security Analysis and Limitations

We analyze the security robustness of DeepVis against adaptive evasion and discuss operational boundaries.

Robustness against Adaptive Evasion. An adversary cognizant of the system might attempt to evade detection by manipulating file attributes. leftmargin=*

- *Low-Entropy Mimicry:* Padding a malicious binary with null bytes lowers entropy (Red channel evasion). However, this creates a *Trilemma*: padding increases file size or alters structure, triggering Context (Green) or Structure (Blue) alarms. Simultaneous minimization of all three signals while maintaining malicious utility is statistically improbable.
- *Hash Collision Targeting:* An attacker might craft filenames to collide with high-churn benign files. DeepVis mitigates this via Max-Risk Pooling, where the highest risk score dominates the pixel value ($T_{x,y} = \max_i \text{Feature}(f_i)$), preventing signal dilution. Furthermore, assuming the secret key K is protected via ephemeral session generation or privileged memory restrictions, the adversary cannot predict target coordinates.
- *Contextual Masking:* Hiding a rootkit in a safe path lowers the Context score but exposes Structural anomalies (e.g., a kernel module in /usr/bin). The feature orthogonality ensures that masking one dimension amplifies anomalies in others.

Operational Limitations. DeepVis prioritizes hyperscale throughput via header-only sampling (first 128 bytes). While this covers 96% of active binary threats (Section IV-B), it inherently misses deep-payload injections in script-based attacks or polyglots. This design reflects a deliberate trade-off: deep-payload scanning at hyperscale is computationally infeasible for continuous monitoring. Thus, DeepVis functions as a *High-Frequency Triage Filter*, drastically reducing the search space from 100% of files to 0.6% of flagged artifacts. This enables heavier forensic tools (e.g., full-content analyzers, memory forensics) to focus exclusively on high-risk targets, trading theoretical completeness for operational feasibility. Additionally, memory-resident threats (e.g., ptrace injections) leave no disk footprint and require complementary memory forensics.

Deployment and Key Security. The integrity of the spatial mapping relies on the secrecy of the HMAC key K. In high-security deployments, K should be managed by a Trusted Execution Environment (TEE) or Hardware Security Module (HSM) to prevent host-side extraction. To minimize the Trusted Computing Base (TCB), DeepVis supports an Agentless Architecture where target snapshots are mounted read-only on a trusted verifier instance, isolating the monitoring process from the potentially compromised host kernel.

VII. Conclusion

In this paper, we design and implement DeepVis, a high-throughput integrity verification framework based on a spatial hash projection architecture. By transforming unordered file systems into fixed-size tensors and integrating local maximum detection, we optimize the detection logic to preserve sparse attack signals against diffuse system updates. We evaluate DeepVis on production infrastructure and show that it achieves an F1-score of 0.96 with zero false positives, surpassing the scalability limits of traditional FIM, and enables 168× more frequent monitoring. This is achieved by decoupling inference complexity from file count and maintaining negligible runtime overhead (+2% P99 latency) through asynchronous I/O pipelining.

References

[1] R. Lehti and P. Virolainen, "AIDE: Advanced Intrusion Detection Environment," https://aide.github.io, 1999.

[2] G. H. Kim and E. H. Spafford, "The design and implementation of Tripwire: A File System Integrity Checker," in *Proceedings of the 2nd ACM Conference on Computer and Communications Security (CCS)*, 1994, pp. 18–29.

[3] The Falco Project, "Falco: Cloud Native Runtime Security," https://falco.org, 2016.

[4] D. B. Cid, "OSSEC: Open Source Host-based Intrusion Detection System," https://www.ossec.net, 2008.

[5] D. Arp, E. Quiring, F. Pendlebury, A. Warnecke, F. Pierazzi, C. Wressnegger, L. Cavallaro, and K. Rieck, "Dos and Don'ts of Machine Learning in Computer Security," in *Proceedings of the 31st USENIX Security Symposium*, 2022, pp. 1345–1362.

[6] I. Cisco Systems, "ClamAV: The Open Source Antivirus Engine," https://www.clamav.net, 2002.

[7] X. Han, T. Pasquier, A. Bates, J. Mickens, and M. Seltzer, "UNICORN: Runtime Provenance-Based Detector for Advanced Persistent Threats," in *Proceedings of the 27th Annual Network and Distributed System Security Symposium (NDSS)*, 2020.

[8] M. Zaheer, S. Kottur, S. Ravanbakhsh, B. Poczos, R. R. Salakhutdinov, and A. J. Smola, "Deep sets," in *Advances in Neural Information Processing Systems*, vol. 30, 2017.

[9] R. Wichmann, "Samhain: File Integrity Checker," https://www.la-samhna.de/samhain/, 2003.

[10] Z. Cheng, Q. Lv, J. Liang, Y. Wang, D. Sun, T. Pasquier, and X. Han, "Kairos: Practical intrusion detection and investigation using whole-system provenance," in *IEEE Symposium on Security and Privacy (S&P)*, 2024.

[11] Y. He *et al.*, "Cross Container Attacks: The Bewildered eBPF on Clouds," in *Proceedings of the 32nd USENIX Security Symposium*, 2023.

[12] TFJMP Contributors, "Hardware-assisted Defense-in-depth for eBPF Kernel Extensions," in *Proceedings of the 2024 CCS Cloud Computing Security Workshop (CCSW)*, 2024.

[13] L. Nataraj, S. Karthikeyan, G. Jacob, and B. S. Manjunath, "Malware Images: Visualization and Automatic Classification," in *Proceedings of the 4th Workshop on Visualization for Cyber Security (VizSec)*, 2011, pp. 1–7.

[14] G. Conti, E. Dean, M. Sinda, and B. Sangster, "Visual Reverse Engineering of Binary and Data Files," in *Proceedings of the 5th Workshop on Visualization for Cyber Security (VizSec)*, 2008, pp. 1–7.

[15] A. Aldini *et al.*, "Image-based Detection and Classification of Android Malware using CNN-LSTM Hybrid Models," in *Proceedings of the 2024 Annual Computer Security Applications Conference (ARES)*, Vienna, Austria, 2024.

[16] R. Lyda and J. Hamrock, "Using Entropy Analysis to Find Encrypted and Packed Malware," *IEEE Security & Privacy Magazine*, vol. 5, no. 2, pp. 40–45, 2007.

[17] X. Ling *et al.*, "A Wolf in Sheep's Clothing: Practical Black-box Adversarial Attacks for Evading Learning-based Windows Malware Detection," in *Proceedings of the 33rd USENIX Security Symposium*, 2024.

[18] R. Uetz *et al.*, "Detecting Evasions of SIEM Rules in Enterprise Networks," in *Proceedings of the 33rd USENIX Security Symposium*, 2024, pp. 1–18.

[19] M. Du, F. Li, G. Zheng, and V. Srikumar, "DeepLog: Anomaly Detection and Diagnosis from System Logs through Deep Learning," in *Proceedings of the 2017 ACM SIGSAC Conference on Computer and Communications Security (CCS)*, 2017, pp. 1285–1298.

[20] Y. Mirsky, T. Doitshman, Y. Elovici, and A. Shabtai, "Kitsune: An Ensemble of Autoencoders for Online Network Intrusion Detection," in *Proceedings of the 25th Annual Network and Distributed System Security Symposium (NDSS)*, 2018.

[21] L. Ruff *et al.*, "Deep One-Class Classification," in *Proceedings of the 35th International Conference on Machine Learning (ICML)*, 2018, pp. 4390–4399.

[22] S. Akcay, A. Atapour-Abarghouei, and T. P. Breckon, "GANomaly: Semi-Supervised Anomaly Detection via Adversarial Training," in *Proceedings of the 14th Asian Conference on Computer Vision (ACCV)*, 2018.

[23] B. Zong *et al.*, "Deep Autoencoding Gaussian Mixture Model for Unsupervised Anomaly Detection," in *Proceedings of the 6th International Conference on Learning Representations (ICLR)*, 2018.

[24] Y. Su *et al.*, "Robust Anomaly Detection for Multivariate Time Series," in *Proceedings of the 25th ACM SIGKDD Conference on Knowledge Discovery and Data Mining (KDD)*, 2019, pp. 1417–1426.

[25] H. Xu *et al.*, "Unsupervised Anomaly Detection via Variational Auto-Encoder for Seasonal KPIs in Web Applications," in *Proceedings of the 27th World Wide Web Conference (WWW)*, 2018, pp. 187–196.